

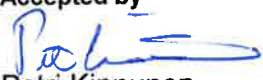


SAFIR2014 – Pipe break analysis: Preliminary leak before break investigation of a steam generator primary collector

Authors: Mikko Patalainen, Heikki Keinänen

Confidentiality: Public

Report's title	
SAFIR2014 – Pipe break analysis: Preliminary leak before break investigation of a steam generator primary collector	
Customer, contact person, address	Order reference
State Nuclear Waste Management Fund (VYR), Fortum Oyj, Technical Research Centre of Finland (VTT)	
Project name	Project number/Short name
FAR2013 – 2.1 Pipe break analysis	81626 – 2.1
Author(s)	Pages
Mikko Patalainen, Heikki Keinänen	28/
Keywords	Report identification code
LBB, steam generator, collector, fracture, leak rate	VTT-R-00578-14
Summary	
<p>This report summarises a preliminary leak before break (LBB) analysis of a dissimilar weld of a steam generator primary collector. The collector contains two different materials: 22K and 08X18H10T steels. During operation the collector is subjected to both thermal and mechanical loads. The operation temperatures rise in the steamer and inlet pipes up to 300 °C and cause thermal stresses in the structure. Mechanical load are caused by the internal pressure in the steam generator.</p> <p>A three dimensional finite element model was generated for fracture mechanics assessment as a part of the leak before break assessment. In the LBB investigation the J-integrals were computed and the leak rate with different crack sizes was studied. Three different cases were modelled: through wall circumferential cracks with sizes of 22.5°, 45° and 67.5° were studied. The rectangular cracks at the dissimilar weld were assumed to be located at the material interface. Also a stress analysis was carried out for a solid unflawed collector model in order to study the stresses in the structure during operation. Analyses were carried out using commercial finite element program Abaqus/Standard with elastic-plastic (ideal plasticity) material properties.</p> <p>Stress distribution results indicated that axial tensile stresses were obtained at the collector internal surface, which may have caused circumferential cracks to occur. J-integrals obtained in from computation were relative low. The leak rate calculations showed that the minimum detectable leak rate can be exceeded only with the circumferential crack sizes higher than 55°. The LBB analysis will be continued in 2014 utilising the available material parameters.</p>	
Confidentiality	Confidential
Espoo 31.1.2014 Written by  Mikko Patalainen Research Scientist	Reviewed by  Juha Kuutti Research Scientist
Accepted by  Petri Kinnunen Deputy Head of Research Area	
VTT's contact address	
Distribution (customer and VTT) VTT, Fortum Oyj	
<i>The use of the name of the VTT Technical Research Centre of Finland (VTT) in advertising or publication in part of this report is only permissible with written authorisation from the VTT Technical Research Centre of Finland.</i>	

Preface

The preliminary fracture mechanics analysis of a steam generator collector done in this study was carried out under research project Fracture assessment of reactor circuit (FAR) task 2.1 "Pipe break analysis". The project concerns integrity of the reactor circuit and its components from computational fracture mechanics point of view. The project is a part of The Finnish Research Programme on Nuclear Power Plant Safety SAFIR2014, which is a national nuclear energy research program. The work in 2013 was funded by the State Nuclear Waste Management Fund (VYR), Fortum Oyj and the Technical Research Centre of Finland (VTT). The work was carried out at VTT.

Espoo 31.1.2014

Authors

Contents

Preface.....	2
Contents.....	3
1. Introduction.....	4
2. Primary steam collector of a VVER440 power plant.....	4
3. Materials.....	5
4. Finite element model.....	6
5. Loads, boundary conditions and constraints.....	8
5.1 Thermal conditions during operation.....	8
5.2 Mechanical loads.....	9
5.3 Boundary conditions and constraints.....	9
6. Computation results.....	10
6.1 Steam collector during operation.....	10
6.2 LBB evaluation.....	14
6.2.1 J-integral stability analysis.....	14
6.2.2 Leak rate evaluation.....	17
7. Summary and conclusions.....	18
References.....	20
Appendices.....	21
A1. Stress linearization of radial and circumferential stress components.....	21
A3. J-integrals.....	22
A3. Crack opening displacements on crack edges.....	24

1. Introduction

This report summarises a preliminary leak before break (LBB) analysis of a dissimilar weld of a steam generator primary collector. The main emphasis of the work is to determine crack severity, calculate leak rates with the assumed through-wall crack sizes and also study occurring stresses and possibility of plastic collapse in the dissimilar weld between the collector nozzle and the steam generator during operation.

In this work thermal and mechanical analyses are carried out for the primary steam collector. The purpose of the study is to evaluate integrity of the structure during operational conditions. During the operation temperatures rise in the steamer and inlet pipes up to 300 °C and cause thermal stresses in the structure. Mechanical load are caused by the internal pressure in the steam generator (44 bar) and the collectors (123 bar). Analyses are carried out using commercial finite element program Abaqus/Standard [1] with elastic-plastic (ideal plasticity) material properties.

2. Primary steam collector of a VVER440 power plant

Figure 1 shows the cross-section view of the steamer of a VVER440 power plant, the two primary collectors and the coolant inlet and outlet pipes. The dissimilar material interface (i.e., weld) is highlighted in green.

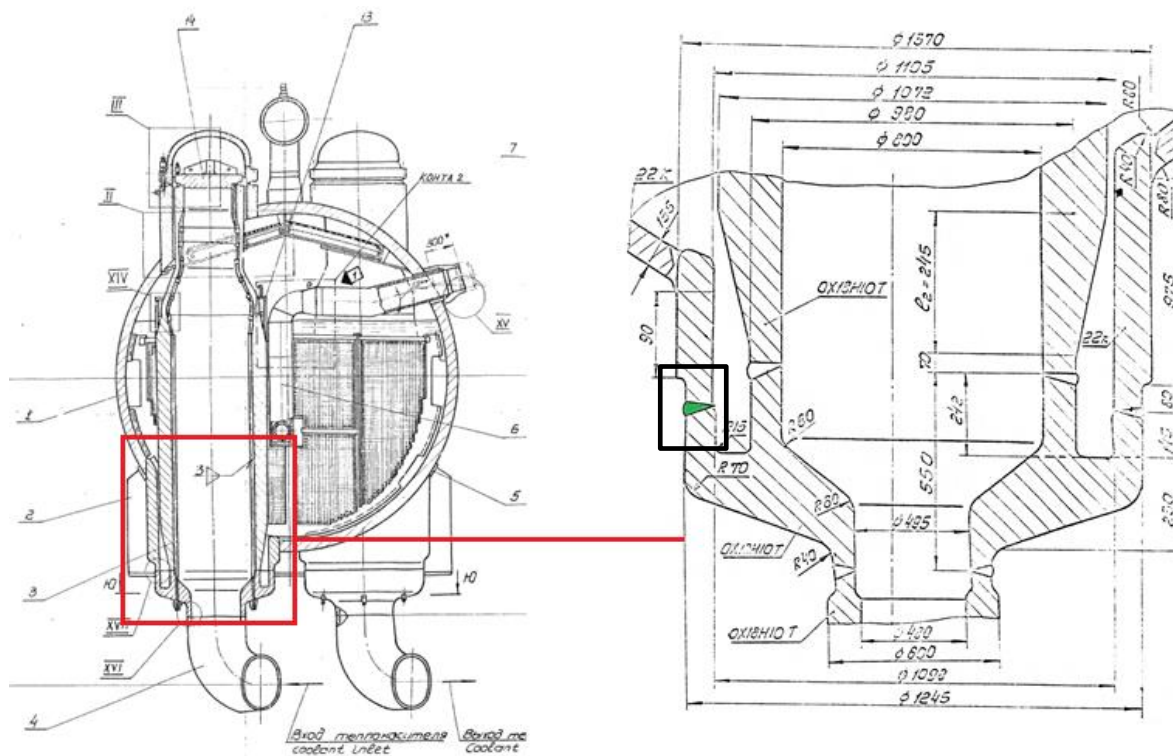


Figure 1. A cross-section view of the steamer of a VVER440 power plant and the primary steam collector. Dissimilar material interface (i.e., weld) is shown in green in the drawing.

3. Materials

The collector contains two different materials: 22K and 08X18H10T steels. Table 1 shows the temperature depended material properties utilised in the computation [2]. Ideally plastic behaviour was assumed for both materials.

Table 1. Material properties for steels 22K and 08X18H10T [2].

	08X18H10T	22K
poisson`s ratio	0,3	0,3
density	7800 kg/m ³	7800 kg/m ³
elastic modulus	205000 MPa	200000 MPa
50 °C	202000 MPa	197000 MPa
100 °C	200000 MPa	195000 MPa
150 °C	195000 MPa	192000 MPa
200 °C	190000 MPa	190000 MPa
250 °C	185000 MPa	185000 MPa
300 °C	180000 MPa	180000 MPa
thermal exp. coeff.	16,4E-06 1/°C	11,5E-06 1/°C
100 °C	16,6E-06 1/°C	11,9E-06 1/°C
150 °C	16,8E-06 1/°C	12,2E-06 1/°C
200 °C	17,0E-06 1/°C	12,5E-06 1/°C
250 °C	17,2E-06 1/°C	12,8E-06 1/°C
300 °C	17,4E-06 1/°C	13,1E-06 1/°C
conductivity	0,01846 W/(mm* °C)	0,040 W/(mm* °C)
yield stress		
20 °C	491 MPa	430 MPa
250 °C	397 MPa	421 MPa
300 °C	377 MPa	412 MPa

4. Finite element model

In this work a 180 degree solid 3D-model with symmetric boundary conditions was used in the simulations. Figure 2 shows the geometry of the steam generator collector. The blue colour indicates steel 08X18H10T and the green indicates steel 22K. A full circumferential section of the steam generator was modelled in order to utilise more realistic boundary conditions. Iteration of model geometry was performed as a part of the boundary conditions studies. Results indicated that use of less detailed geometry did not produce realistic deformation of the loaded structure.

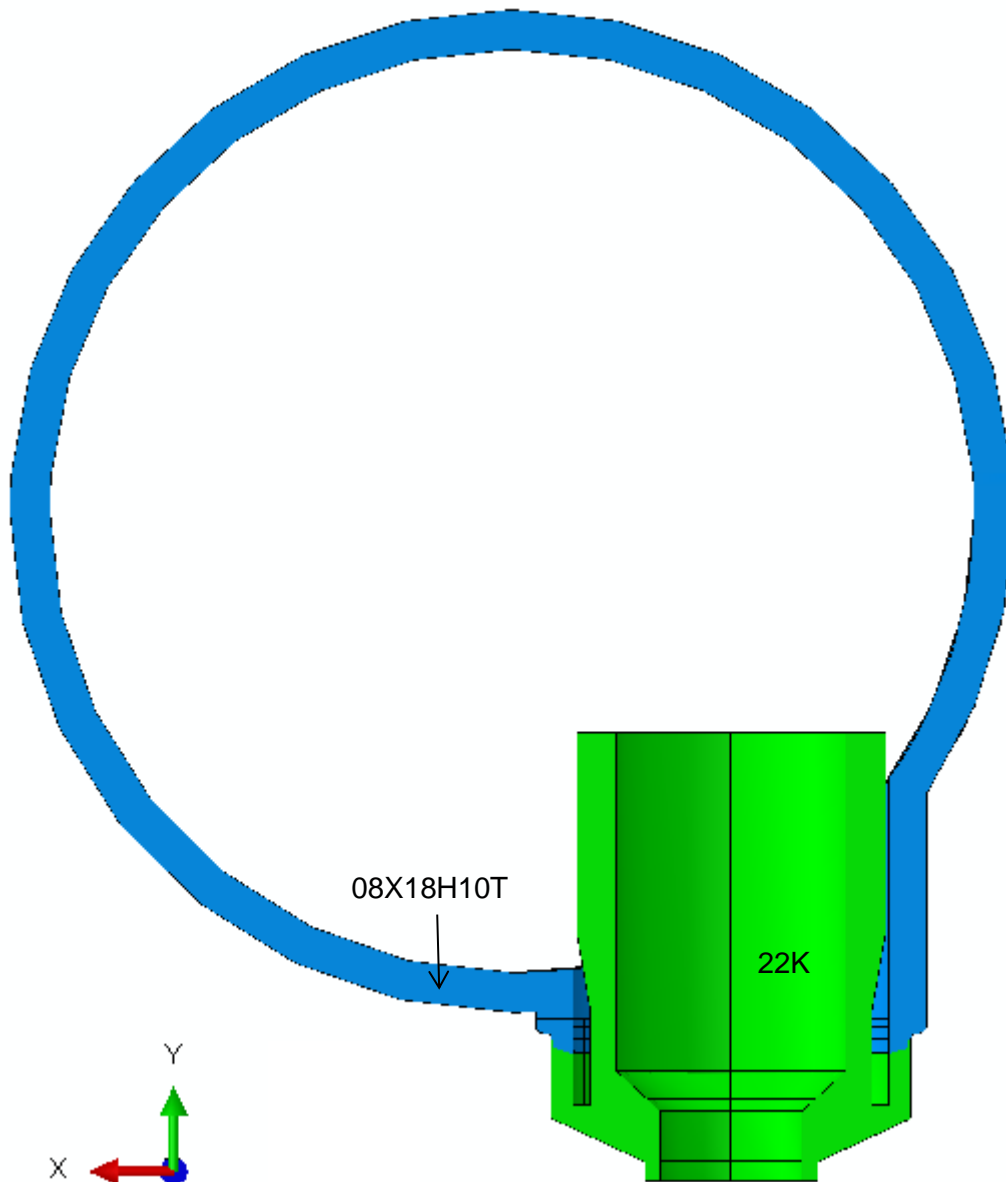


Figure 2. Steam generator collector 180 degree 3D model.

The finite element mesh of the model is shown in Figure 3. The element type used in the analysis is an 20-node quadric brick element with full integration. In Abaqus the element type is called C3D20 [1]. The number of elements in the models varied between 62760 and 63248 the number of nodes varied between 296848 and 299382 depending on the crack model analyzed. The average length of the element was approximately 20 mm.

The FE-model was partitioned also to a smaller section of 90° , which was tied using a “surface-to-surface” constraint. The constraint ties the degrees of freedom of the nearest element nodes located at the surfaces. This part of the model was used for the crack assignment and detailed mesh generation at the crack vicinity. In the computation three different sizes of through-wall cracks were modelled: 22.5° , 45° and 67.5° . Figure 4 shows the mesh in the slice part with circumferential through-wall crack of 22.5° .

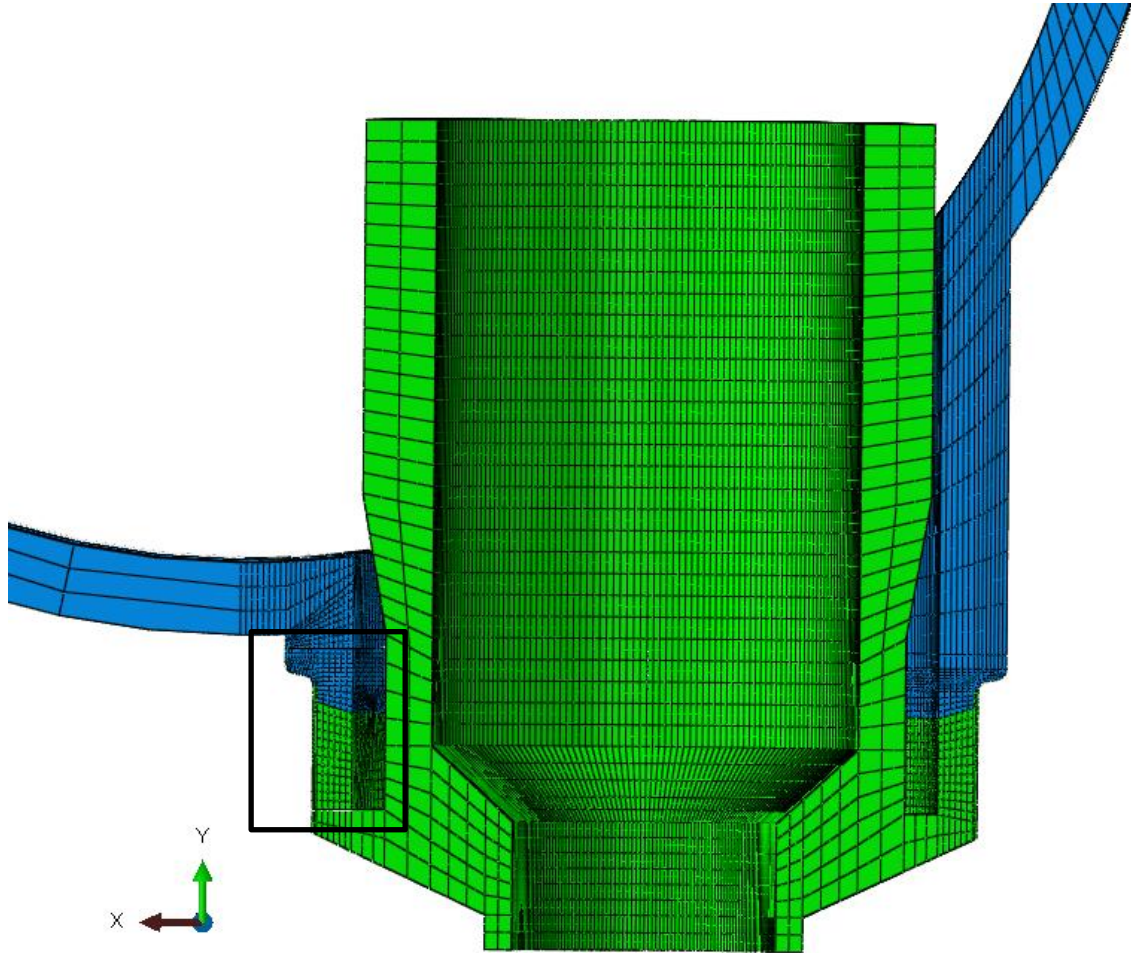


Figure 3. The mesh of the FE-model. A detailed section of 90° was partitioned for crack tip mesh generation (shown below).

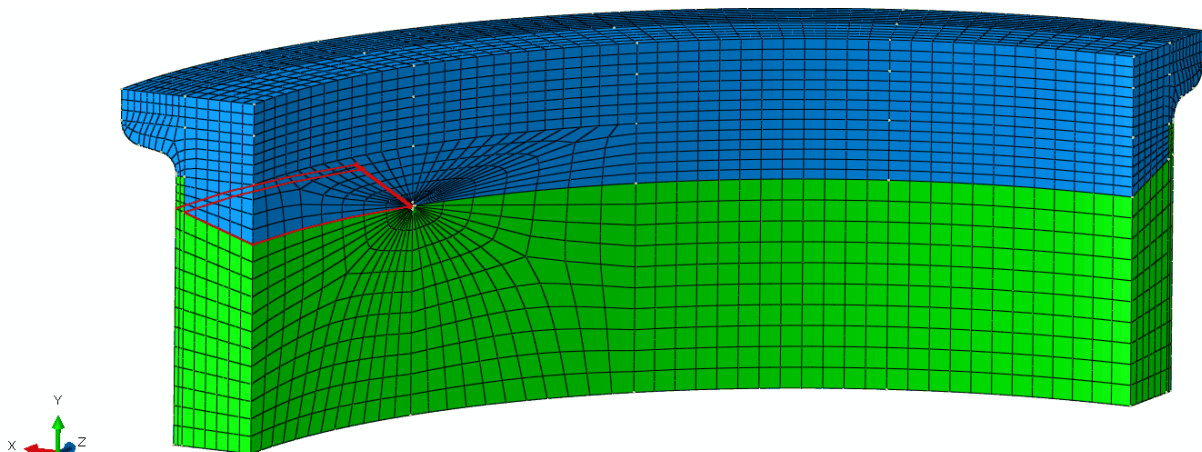


Figure 4. The mesh of a smaller section (90°) with through-wall crack of 22.5° .

5. Loads, boundary conditions and constraints

5.1 Thermal conditions during operation

Thermal loads occur in the structure during operation due to hot water flow into the collector and steam generated in the steamer. Heat is transferred in the structure via conduction and convection. Figure 5 shows the convective surfaces with the equivalent heat transfer coefficients and surrounding temperatures (i.e. sink temperature). It must be noted that the external surfaces of the collector and the steamer are insulated and the temperature at these surfaces was assumed to be 50 °C with extremely low convective heat transfer. Details obtained for the heat transfer analysis are according to the previous work done by Fortum [2].

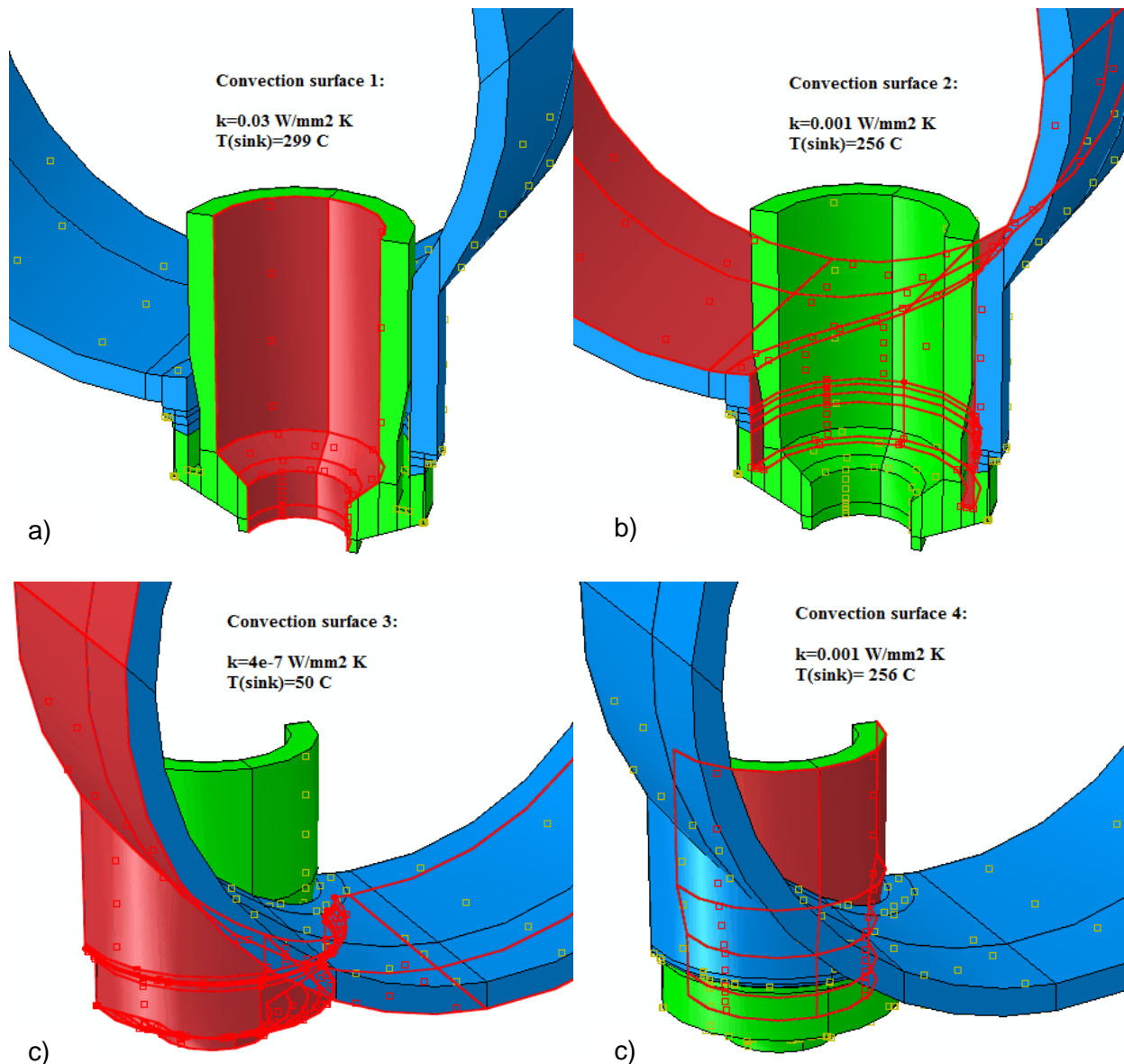


Figure 5. Heat transfer coefficients and sink temperatures utilised in the heat transfer analysis [2].

5.2 Mechanical loads

The physical loads (i.e., internal pressure) and cross-section loads applied in the model are shown in Figure 6 and Figure 7. At the specified surfaces internal pressures of 123 bars and 44 bars were utilised. Cross-section loads were applied at the collector ends and at the steamer cylinder opposite surface. The cross-section loads were calculated from equilibrium equations taking account the cross-section areas and the loading (i.e., internal pressure) during operatio.

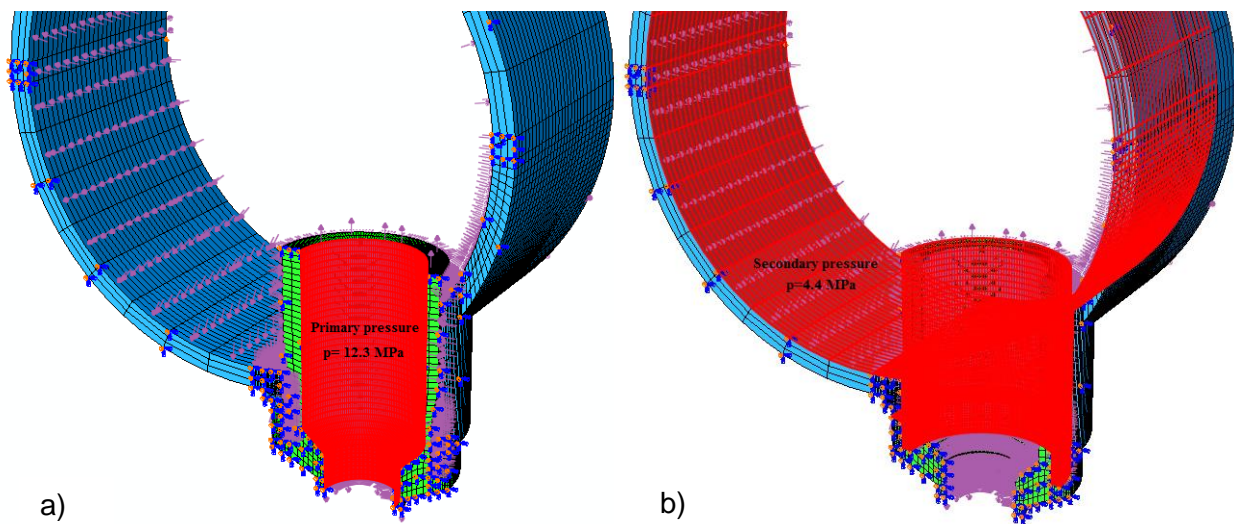


Figure 6. Primary (a) and secondary (b) pressure load in the collector and the steamer.

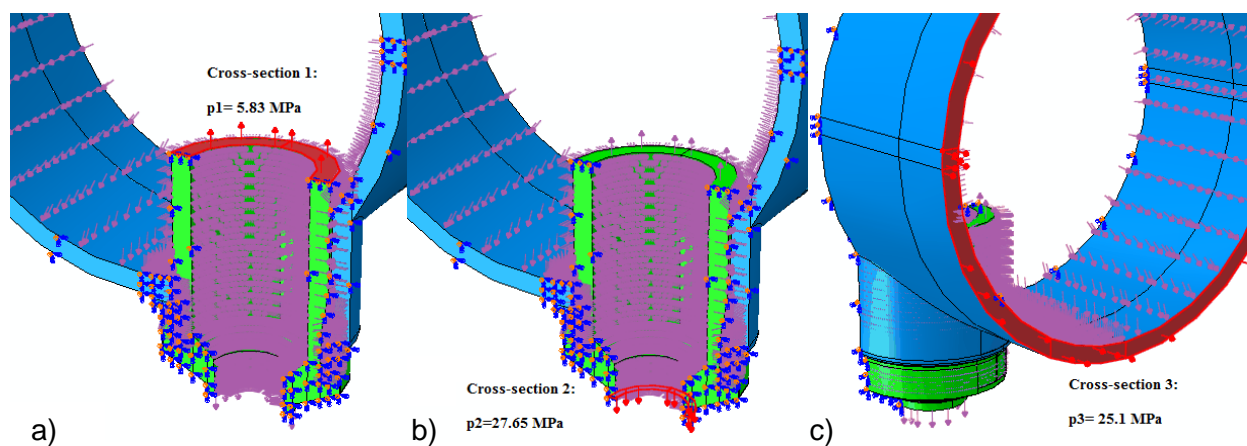


Figure 7. Cross-section loads in the collector and the steamer.

5.3 Boundary conditions and constraints

Due to relatively complex geometry of the steam generator collector it was assumed that the collector cannot be constrained using symmetrical boundary conditions at all surfaces. This would result as unrealistic boundary condition and too stiff structure. The only symmetrical boundary condition was applied at the vertical cross-section of the collector as shown in Figure 8. Also, vertical and horizontal movement was constrained at the opposite end of the steamer in order to constraint free body motion.

In addition to this, cross-section surfaces presented in Figure 7 (above) were constrained to remain in plane preventing warping to occur at the cross-sections.

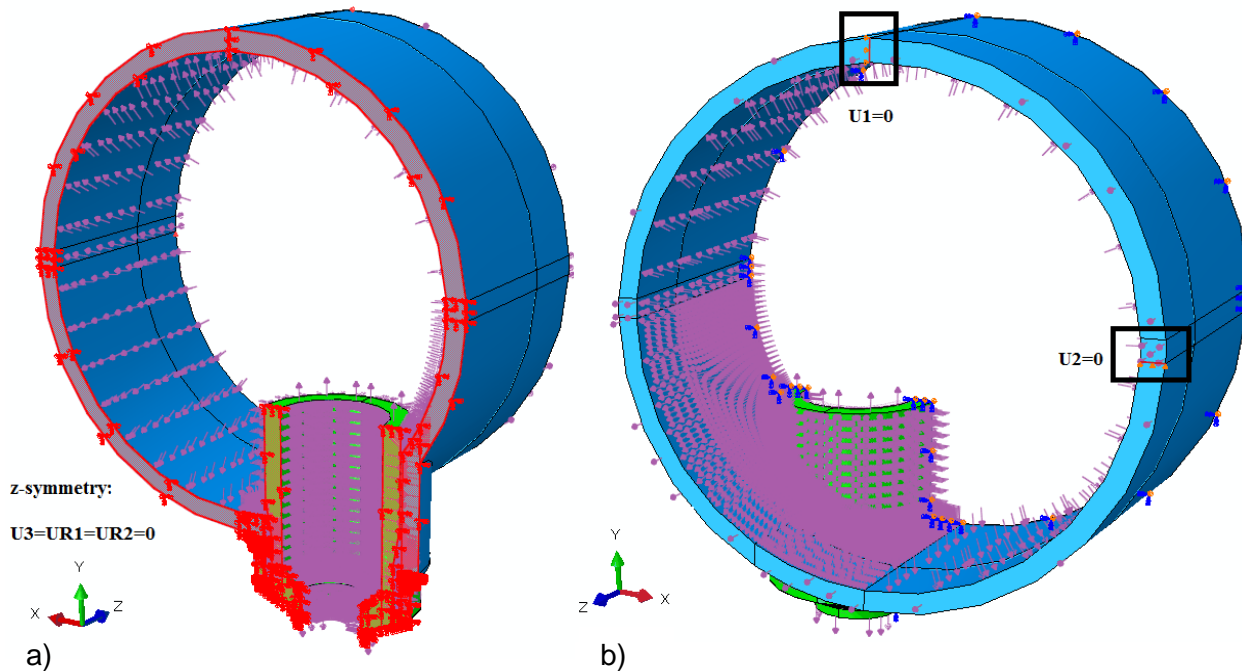


Figure 8. Boundary conditions of the steam generator collector.

6. Computation results

Results of the unflawed (i.e., no crack) steam generator collector model and circumferential through-wall crack cases are presented in this chapter. In the results the axial tensile stresses which can lead to crack initiation are presented. J-integrals are presented in the crack cases.

In addition, leak rate investigation obtained with the SQUIRT2 is presented. The input data (i.e., crack opening shape) for SQUIRT2 computation was obtained from the finite element analyses.

The stress components were obtained from the finite element analyses and linearized in order to determine the average stress (i.e. primary membrane P_m) over the wall thickness. The primary membrane bending stresses were approximated from the stress distribution results obtained in the computation.

Some of the results are listed in the Appendices.

6.1 Steam collector during operation

During operation the collector and the steamer are subjected to both thermal and mechanical loading. Figure 9 shows the temperature distribution of the collector and steamer during operation. The maximum temperature inside the collector rises up to 299 °C and inside the steamer up to 256 °C.

Figure 10 and Figure 11 show the axial tensile stresses in the collector at the dissimilar weld vicinity. The collector tube was removed from the view for clarity. Axial stresses are scaled so that only tensile stresses are presented. Dark areas in the stress distribution indicate compressive stresses.

Results indicated that at the inner surface of the weld peak tensile stresses occur. Tensile stresses with magnitude of more than 200 MPa were obtained. However, it must be noted that at the outer surface of the weld the structure is in compression, according to the

computation. This is mainly due to temperature difference over the wall and also thermal expansion of the materials at the material interface.

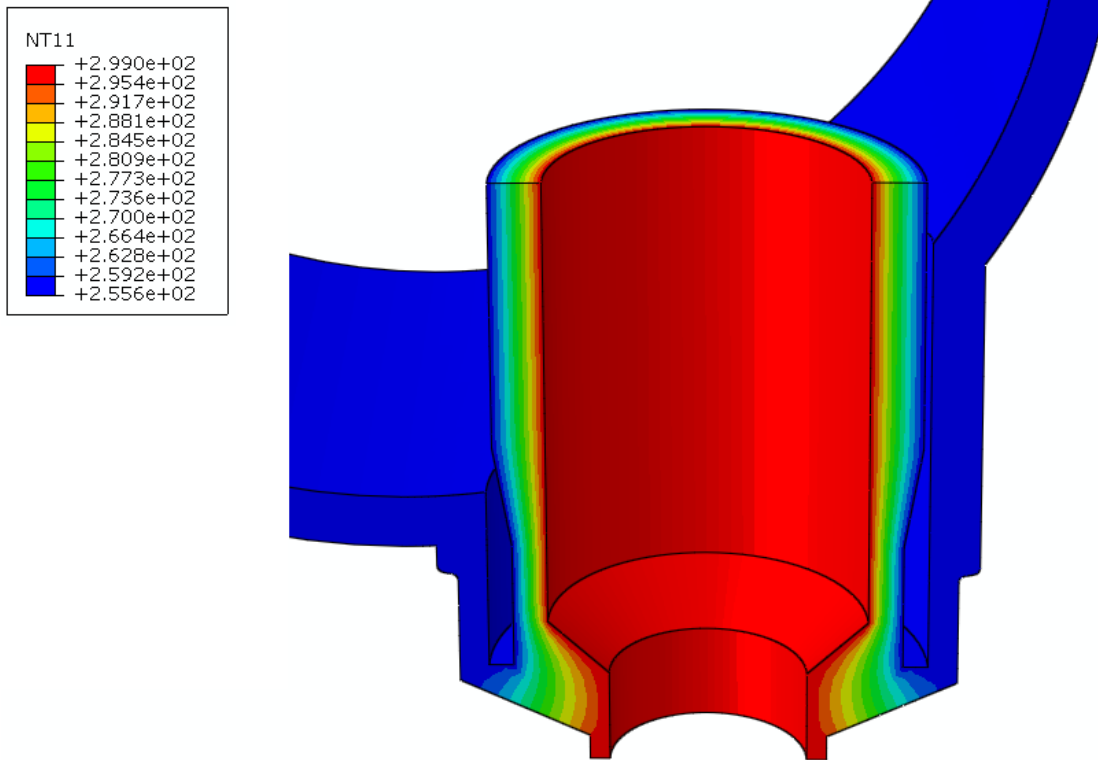


Figure 9. Temperature distribution (°C) in the collector and the steamer.

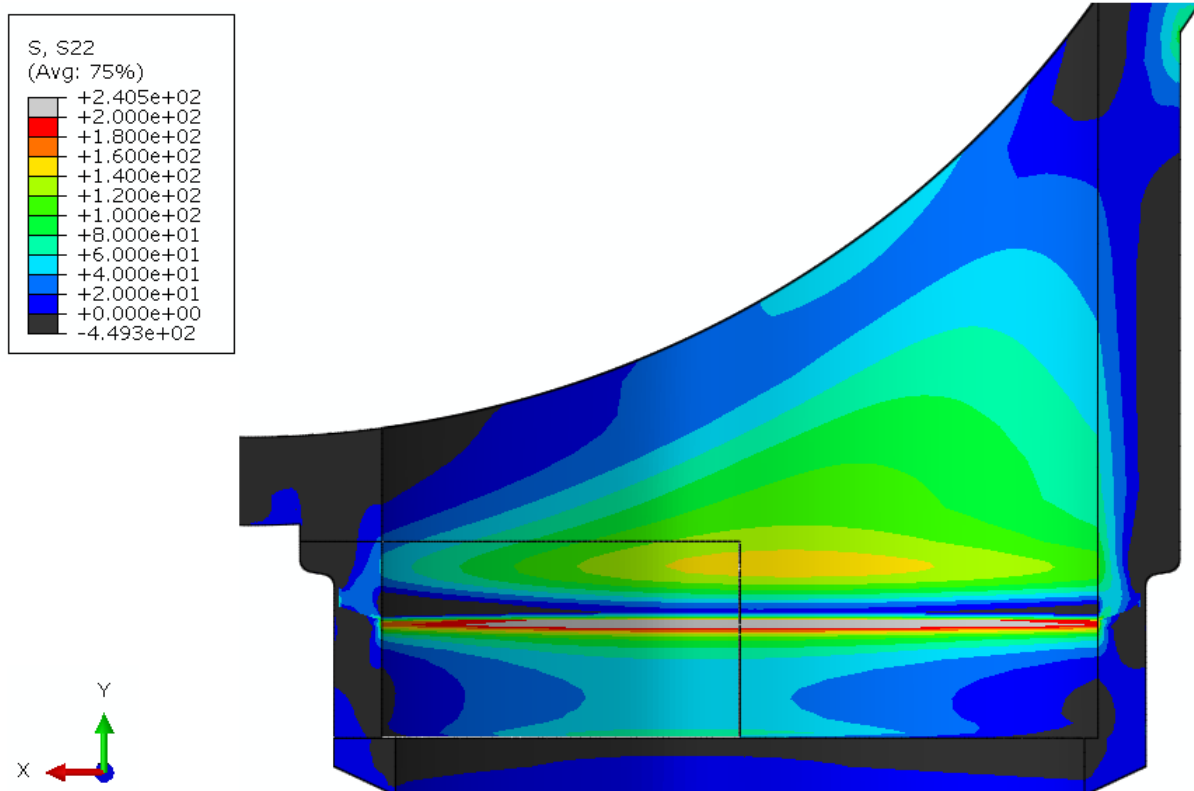


Figure 10. Tensile stress distribution (MPa) in the axial direction of the steam collector.

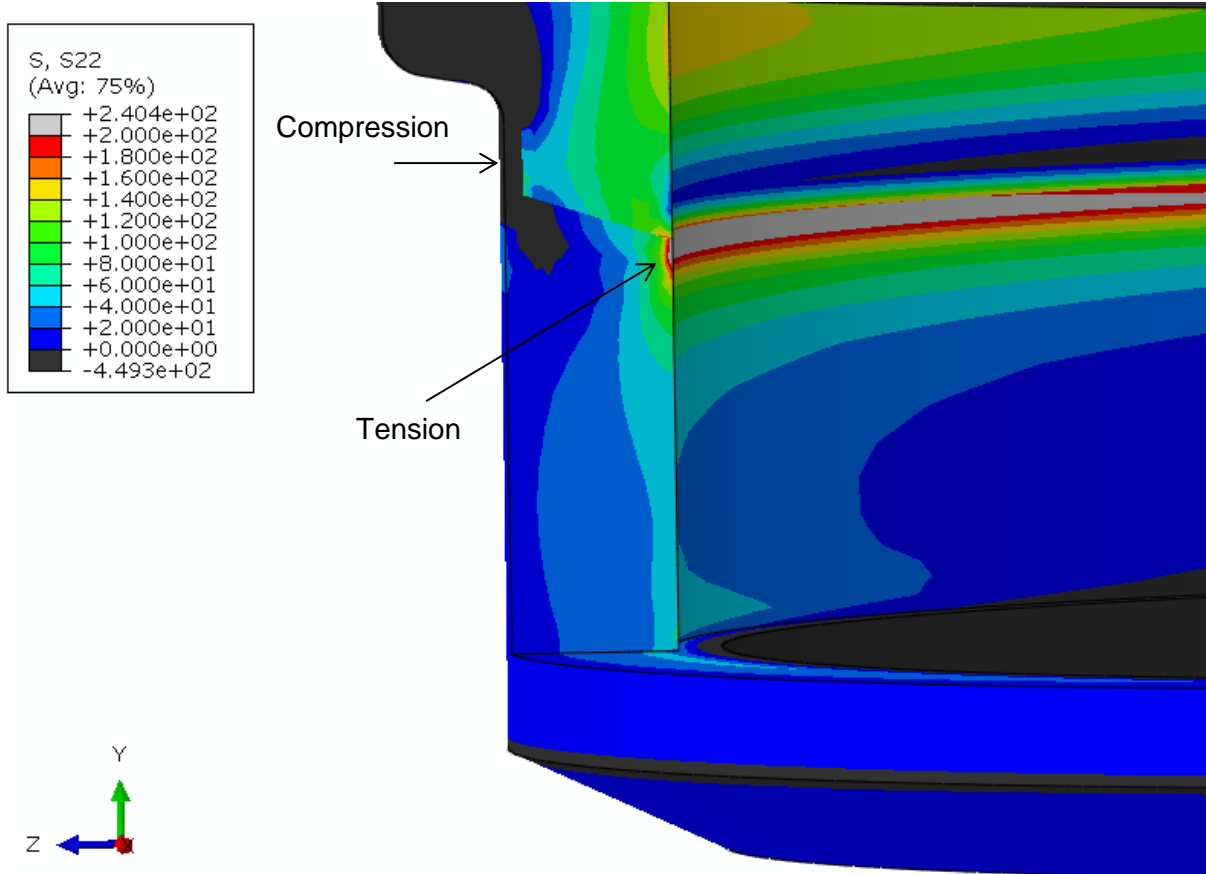


Figure 11. Over the wall tensile stress distribution (MPa) in the axial direction of the steam collector.

Stress linearization was obtained over the wall thickness in order to study occurred primary membrane and bending stresses for stress components. Figure 12 shows the location of the stress linearization path over the wall thickness. A section of 90° was removed from the model in order to carry out stress linearization at the chosen location.

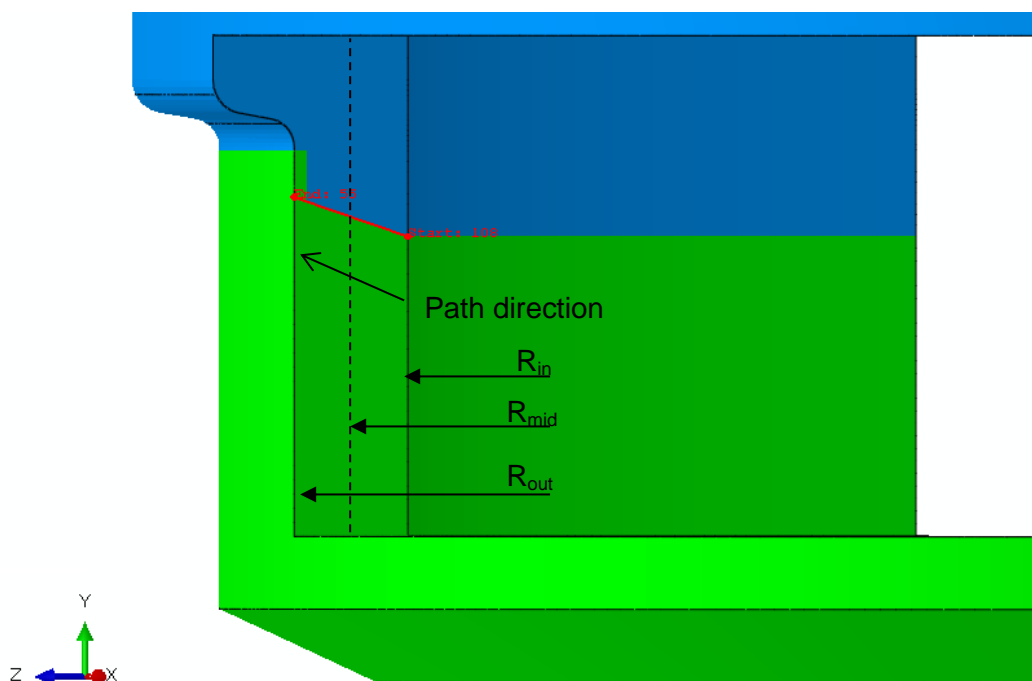


Figure 12. Stress linearization path from inside to outside over the wall thickness.

Figure 13 shows the stress linearization for the axial stress component (S22). The membrane stress (blue line) obtained in the computation was about 49 MPa. The combined membrane+bending (orange line) shows variation of stresses from the internal surface of 105 MPa tension to outside surface of 25 MPa compression.

The stress distributions shown in Figure 10 and Figure 11 together with material yield strength values presented in Table 1 indicate that the possibility of plastic collapse in the component is negligible. This was confirmed by equivalent plastic strain contours obtained from the FE analyses.

Stress linearization of radial and circumferential stress components are shown in Appendix A.



Figure 13. The stress linearization for the axial stress component (S22). Blue line indicates the membrane stress and the orange line indicates the combined membrane+bending stress.

6.2 LBB evaluation

The leak before break (LBB) argument is aimed at demonstrating that leakage of fluid through a crack in the wall of pressure component can be detected prior to the crack reaches instability, which may lead to a catastrophic failure.

The development of a LBB assessment will usually involve some or all of the following to be considered [3]:

- Crack shape development of a part-through-wall flaw as it grows in the through-wall direction by a mechanisms such as fatigue;
- How the flaw eventually breaks through the wall and re-characterises as a through-wall flaw;
- Limiting size of through-wall flaw;
- Crack opening area of through-wall flaws;
- Leakage rate of fluid from through-wall flaws (based on crack opening area/crack gap information);
- Evaluation of detectable leakage flaw size (based on leakage rate and flow detection methods);
- Evaluation of margin between limiting through-wall size and detectable leakage flaw size.

LBB assessment sections highlighted with red were not considered in this work.

In this study the LBB assessment was carried out by three fracture mechanics models with different assumed crack through wall crack sizes, as mentioned earlier. General observations were made about the calculated J-integrals from FE analysis and the crack opening sizes from the deformed FE models were used to determine the minimum detectable leak rate.

6.2.1 J-integral stability analysis

J-integrals were obtained from the crack analyses. Integration over ten integration paths (i.e., contours) was performed for the J-integral estimations at the crack front. Figure 14 shows the results of J-integrals with different crack sizes. The values shown in Figure 14 were obtained by calculating average values at three different locations (i.e., R_{in} , R_{mid} and R_{out} as shown in Figure 12) at the crack front in the direction of wall thickness. Results show that J-integral value variation was obtained and the values are not directly comparable with different crack sizes at locations R_{in} , R_{mid} and R_{out} . Results indicated also that the bigger the crack size the higher values of J-integrals were obtained. However, J-integrals obtained from the analyses were relatively low by a magnitude.

It was also noted that the cracks were not opened purely in axial direction (i.e., K_I mode) but also some rotation towards centroid was obtained (i.e., combination of K_I and K_{III} was obtained). Figure 15 shows the deformed structure (scaled by a factor of 100) and the crack opening shape in the 45° crack model. Nearly similar deformation was obtained also in 22.5° and 67.5° crack models.

Figure 16 shows the stress distributions in the axial direction in each crack analysis. Results indicate that crack surfaces are in compression until the crack front and highly in tension at the crack front.

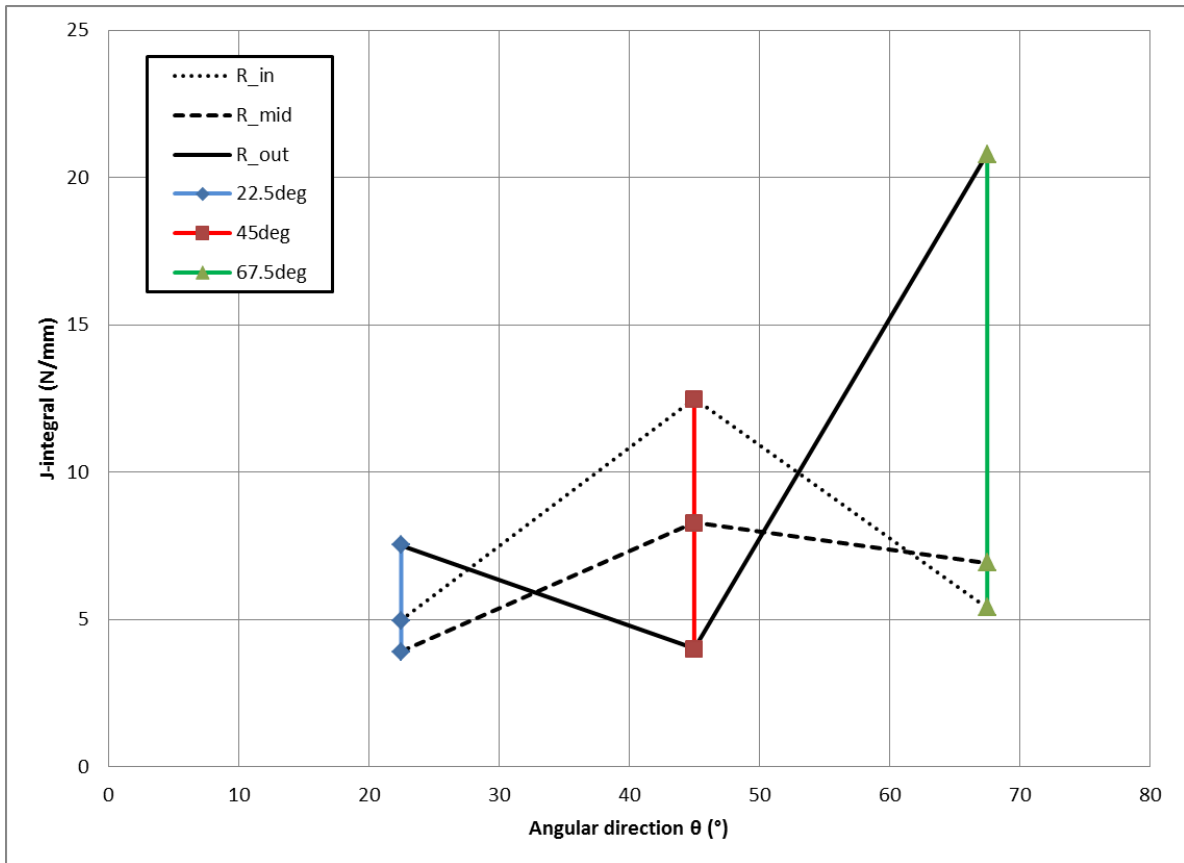


Figure 14. J-integral estimates with different angular crack sizes. R_{in} , R_{mid} and R_{out} indicate the location of the integral paths chosen for the J-integral computation.

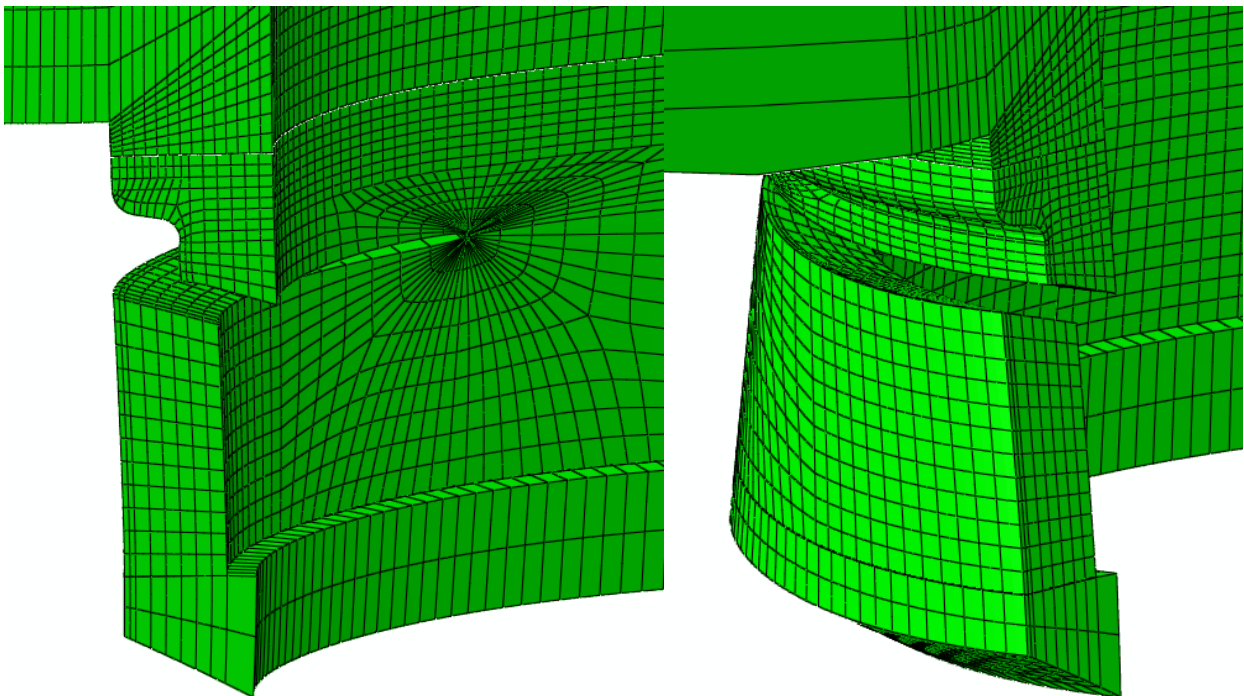


Figure 15. Deformed structure of 45° crack model. Deformation is scaled by a factor of 100.

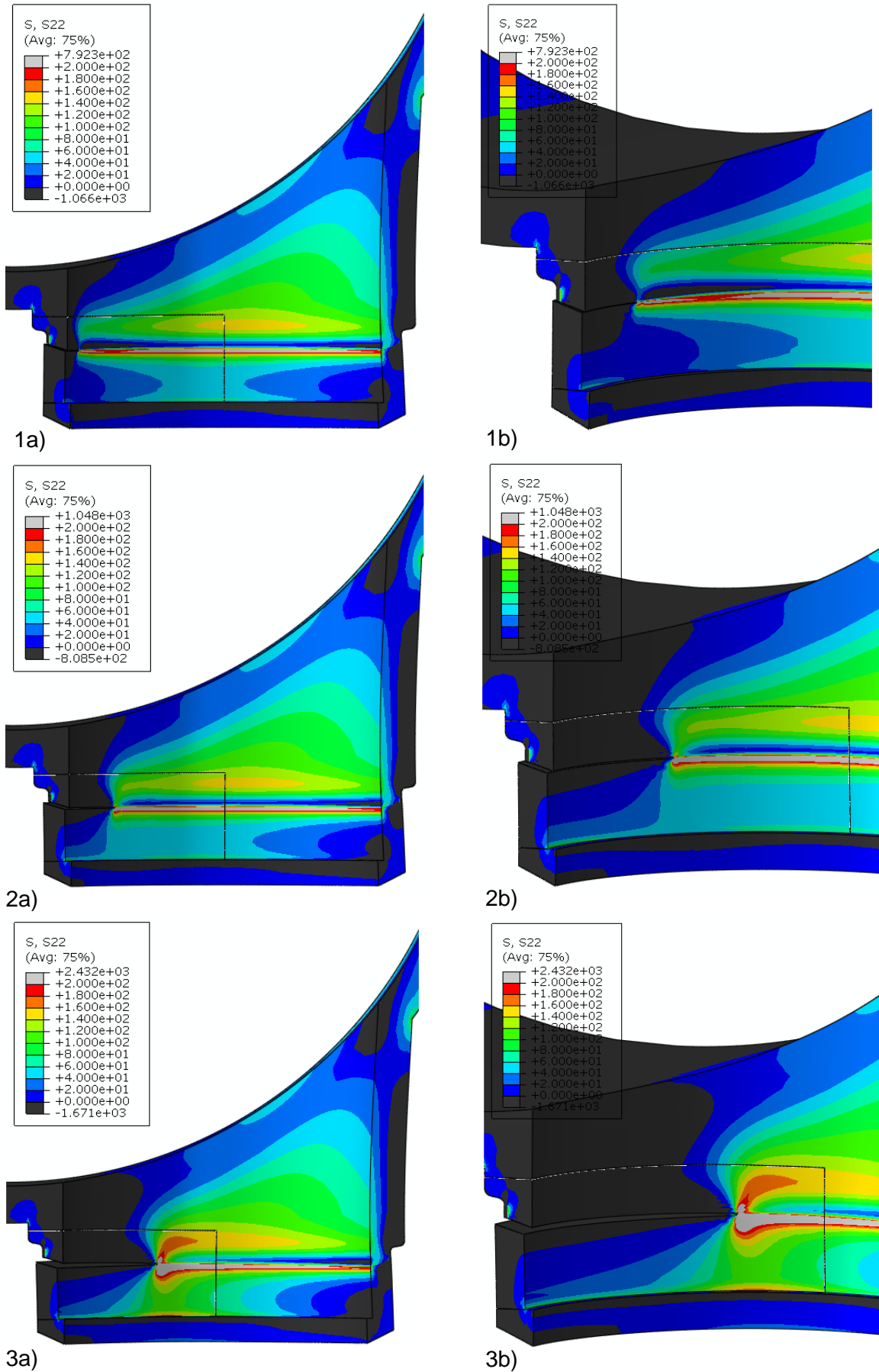


Figure 16. Axial tensile stress distribution at the crack vicinity with crack sizes of 22.5° (1a/b), 45° (2a/b) and 67.5° (3a/b).

6.2.2 Leak rate evaluation

Fluid mass and volume flow rates were calculated using SQUIRT2 code (thermal hydraulics) [4]. In case of thermal hydraulic analysis made by SQUIRT2 the user has to select following options of the program and to make following specifications [5]:

- choose units (either SI or English units),
- choose crack opening shape (diamondshaped, rectangular or elliptic),
- choose type of crack (IGSCC type, fatigue type or other, in case of other the user has to specify the numerical value of surface roughness and pathway loss coefficient),
- specify fluid thermodynamic state inside the pipe (in case of saturated liquid specify pressure or temperature, in case of sub cooled liquid specify pressure and temperature),
- specify crack depth (usually equal to pipe wall thickness),
- specify the average length of the crack,
- specify exterior gap (the crack opening displacement on the outside of the pipe at midpoint location),
- specify interior gap and
- specify fluid pressure.

In this case SI units were used. Shape of the crack was chosen as rectangular and the crack type as fatigue. The specific crack shape details (crack depth, length, exterior and interior gap) were chosen according to the FE analyses. Appendix B shows the vertical displacement at the crack opening edges.

Based on the input data provided by the finite element analyses fluid mass and volume flow rates were calculated using SQUIRT2 code. Figure 17 shows the mass flow rate as a function of circumferential crack size. The detectable leak rate imposed by the United States Nuclear Regulatory Commission (USNRC) is shown also in the chart as a part of the methodology of the LBB analysis. The minimum detectable leak rate according to the USNRC is 10 gallon per minute (GPM) [5].

Analysis results indicate that the minimum mass flow rate cannot be detected with angular crack sizes less than $\theta=55^\circ$ when linear interpolation was used. Minimum leak rate of 10 gallon per minute is exceeded only with angular crack sizes of over $\theta=55^\circ$. In this study only the assumed crack size of $\theta=67.5^\circ$ exceeded the minimum leak rate with a by a magnitude of 19.5 gallon per minute.

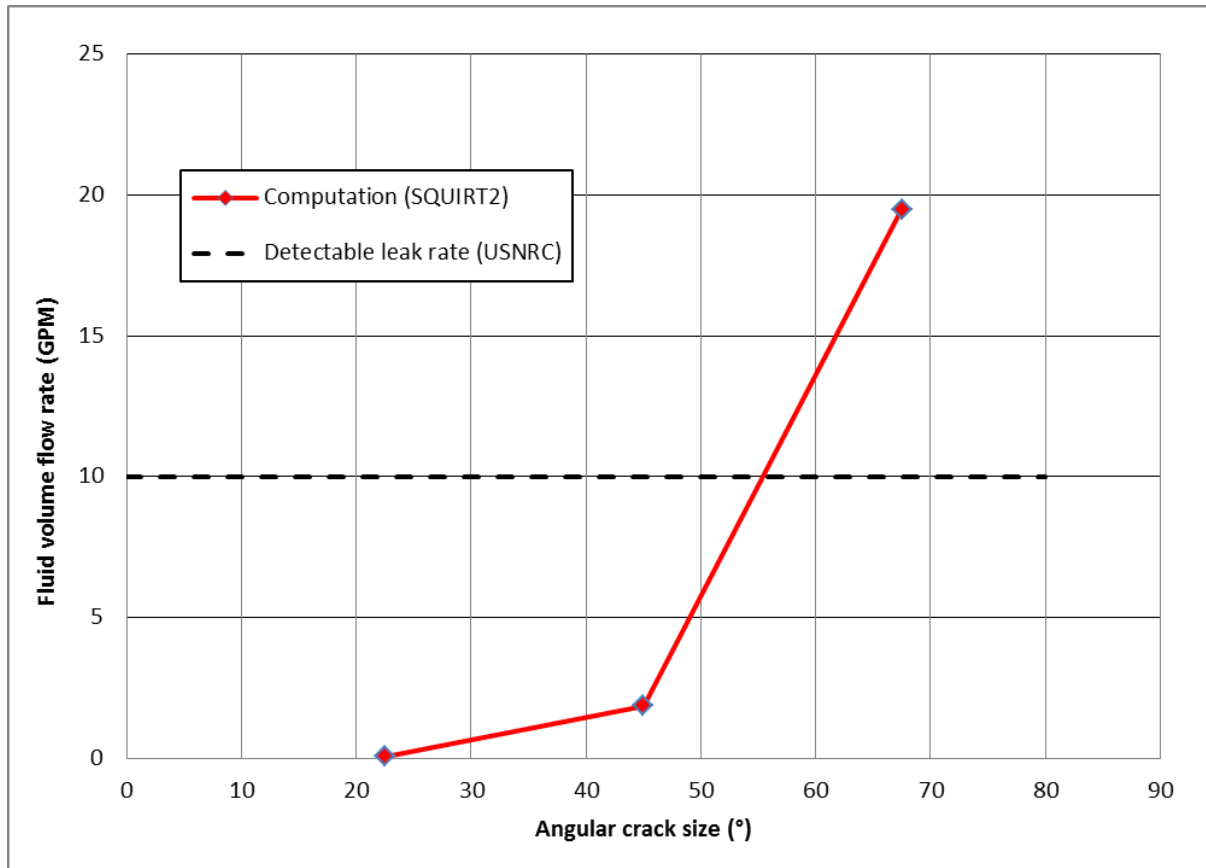


Figure 17. Mass flow rate with crack sizes of 22.5°, 45° and 67.5°.

7. Summary and conclusions

A preliminary LBB analysis was carried out of a dissimilar weld of a steam generator primary collector. The main emphasis of the work is to determine crack severity, calculate leak rates with the assumed through-wall crack sizes and also study occurring stresses in the dissimilar material weld between the collector nozzle and the steam generator during operation. During the operation temperatures rise in the steamer and inlet pipes up to 300 °C and cause thermal stresses in the structure. Mechanical loads are caused by the internal pressure in the steam generator (44 bar) and the collectors (123 bar). Analyses were carried out using commercial finite element program Abaqus/Standard [1] with elastic-plastic (ideal plasticity) material properties.

Results obtained from an unflawed solid steam collector model indicated that axial (i.e., vertical) stresses occurred at the inner surface of the weld. Tensile stresses with magnitude of more than 200 MPa were obtained. However, the stresses over the wall thickness were not entirely pure tension but compression was also observed at the outer surface of the weld. This was assumed to be related mainly due to temperature difference over the wall and thermal expansion of the materials at the material interface.

Fracture model results with different assumed through-wall cracks indicated that J-integrals obtained from the analyses were relative low. It was also observed that the crack loading direction was not purely axial but also sliding between crack surfaces was obtained. This could result to a crack closure in the best case scenario and more over limit the leak rate. The possibility of plastic collapse was observed to be negligible as well.

The leak rate investigation carried out with the SQUIRT2 code indicated that the minimum detectable leak rate (10 GPM) imposed by the USNRC was exceeded only with the angular

crack sizes over approximately $\theta=55^\circ$ when linearly interpolated. Smaller circumferential cracks do not exceed the minimum detectable leak rate. It was also observed that the crack growth direction was not purely axial (i.e., enhancing opening) but also horizontal sliding between crack surfaces was obtained. This could result to a crack closure in the best case scenario and more over limit the leak rate.

According to the J-integral results and the leak rate calculations, the component is at risk of breaking before leak if material fracture toughness is less than about 20 kJ/m^2 (or N/mm).

The work will be continued during 2014 by utilising detailed available material properties.

References

1. ABAQUS 6.13-2, Dassault Systemes Simulia Corp., Rising Sun Mills, 166 Valley Street, Providence, RI 02909-2499, USA.
2. Vehkanen S., Strength analysis of the steam generator bimetallic weld, NUCL-1146, 2002, Fortum Nuclear Services (confidential)
3. Keinänen H. & Cronvall O., Pipe break analysis: An updated state-of-the-art review of LBB procedures with computational examples, VTT report: VTT-R-00299-12, 2012, Espoo
4. SQUIRT Computer Code Version 2.4, User's Manual, International Piping Integrity Research Group Program, Contract NRC-04-91-063, Columbus, OH 43201-2693, 1995
5. Ikonen K., Raiko H. and Keskinen R., Leak-Before-Break Evaluation Procedures for Piping Components, STUK-YTO-TR 83, FINNISH CENTRE FOR RADIATION AND NUCLEAR SAFETY, ISSN 0785-9325, 1995, Helsinki

Appendices

A1. Stress linearization of radial and circumferential stress components

Stress linearization at $\theta=90^\circ$ along material interface, through wall.

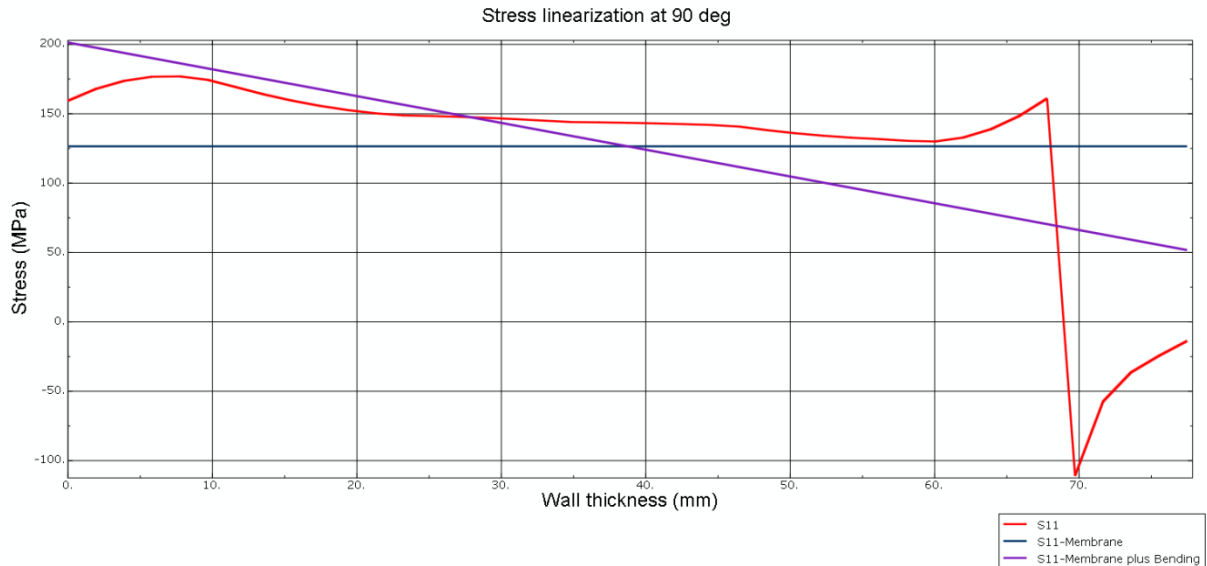


Figure 18. The stress linearization for the radial stress component (S_{11}). Blue line indicates the membrane stress and the purple line indicates the combined membrane+bending stress.



Figure 19. The stress linearization for the circumferential stress component (S_{33}). Brown line indicates the membrane stress and the green line indicates the combined membrane+bending stress.

A3. J-integrals

Figures below show the J-integrals estimated from 5 integration paths (contours) at three locations: R_in, R_mid and R_out. Also the average value obtained from the contours is shown.

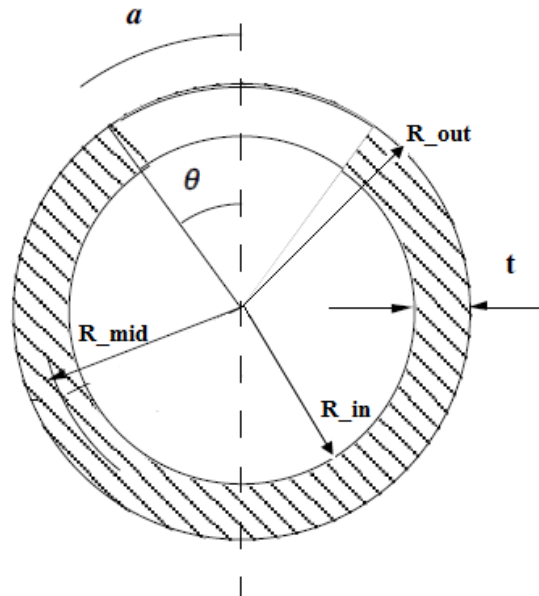


Figure 20. Schematic view of the tube cross-section and through wall crack.

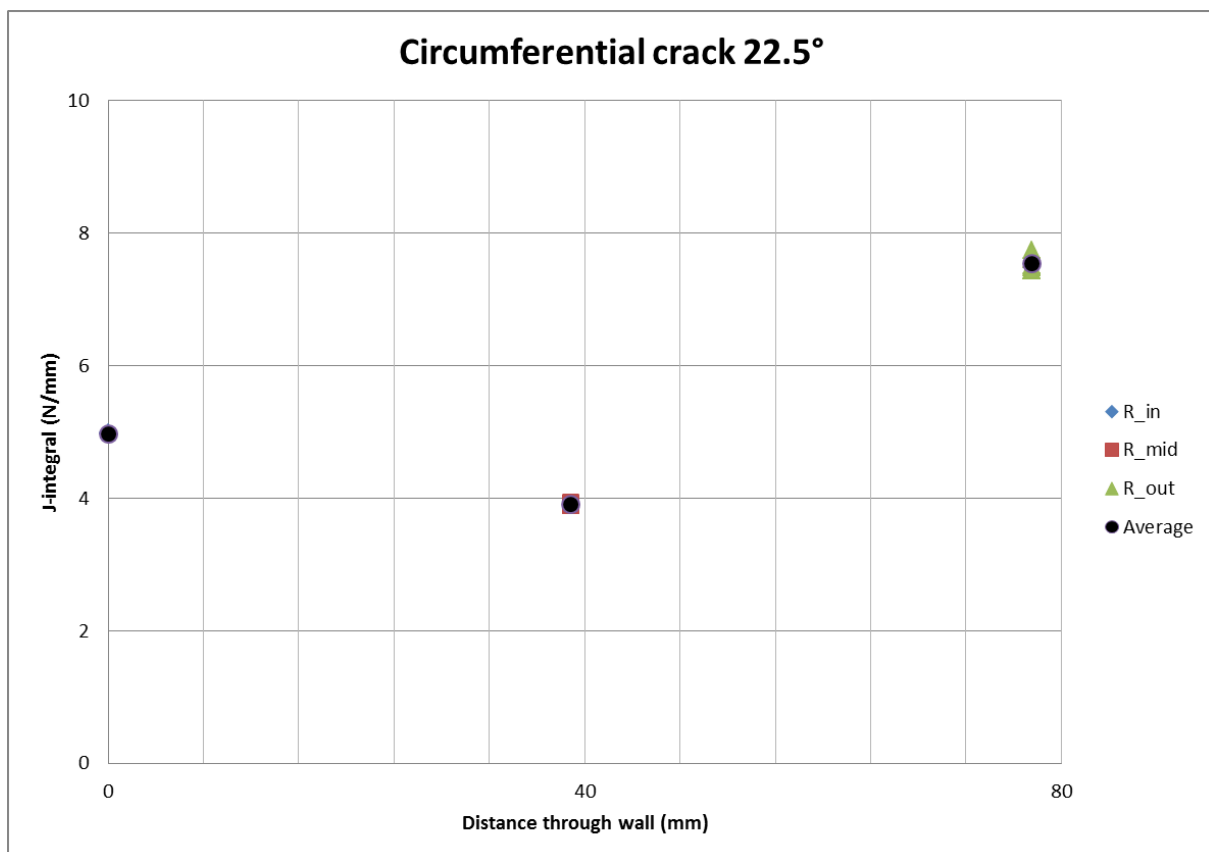


Figure 21. Calculated J-integrals from the $\theta=22.5^\circ$ crack.

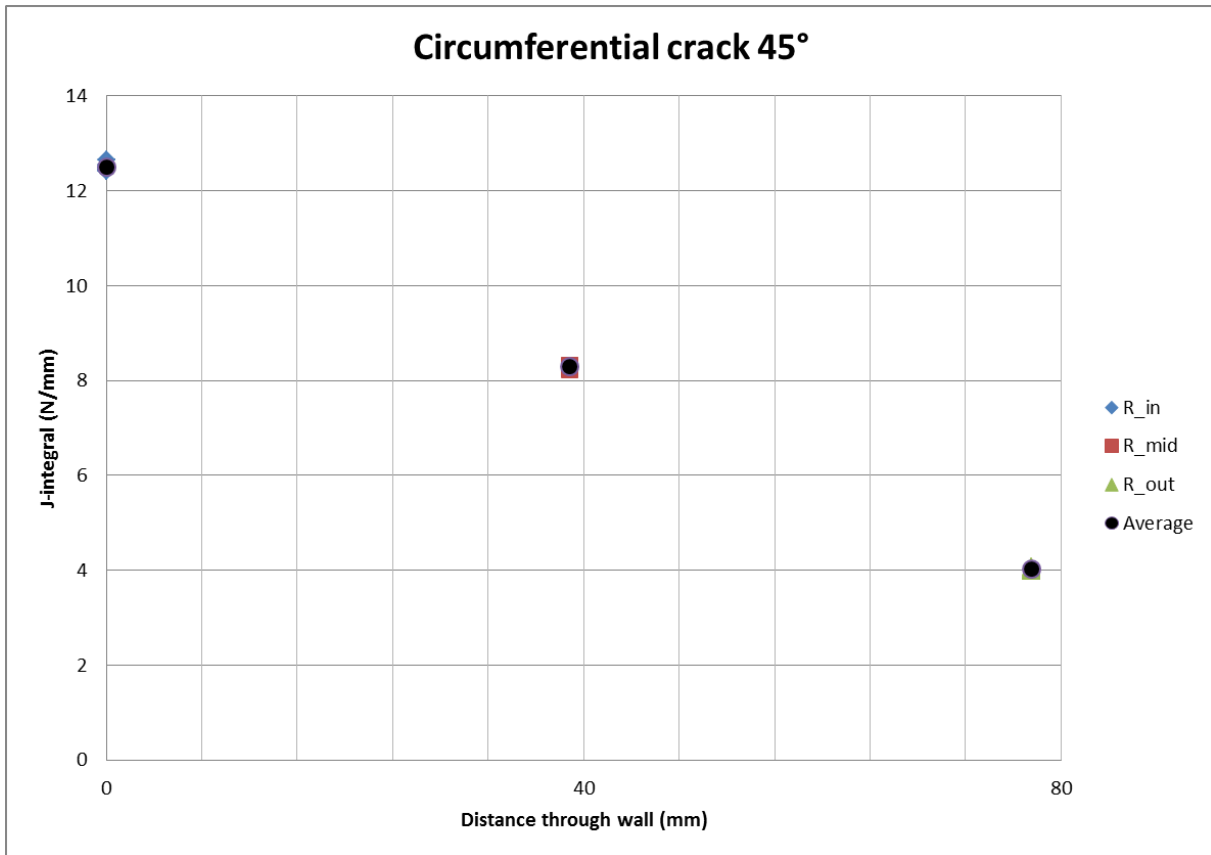


Figure 22. Calculated J-integrals from the $\theta=45^\circ$ crack.

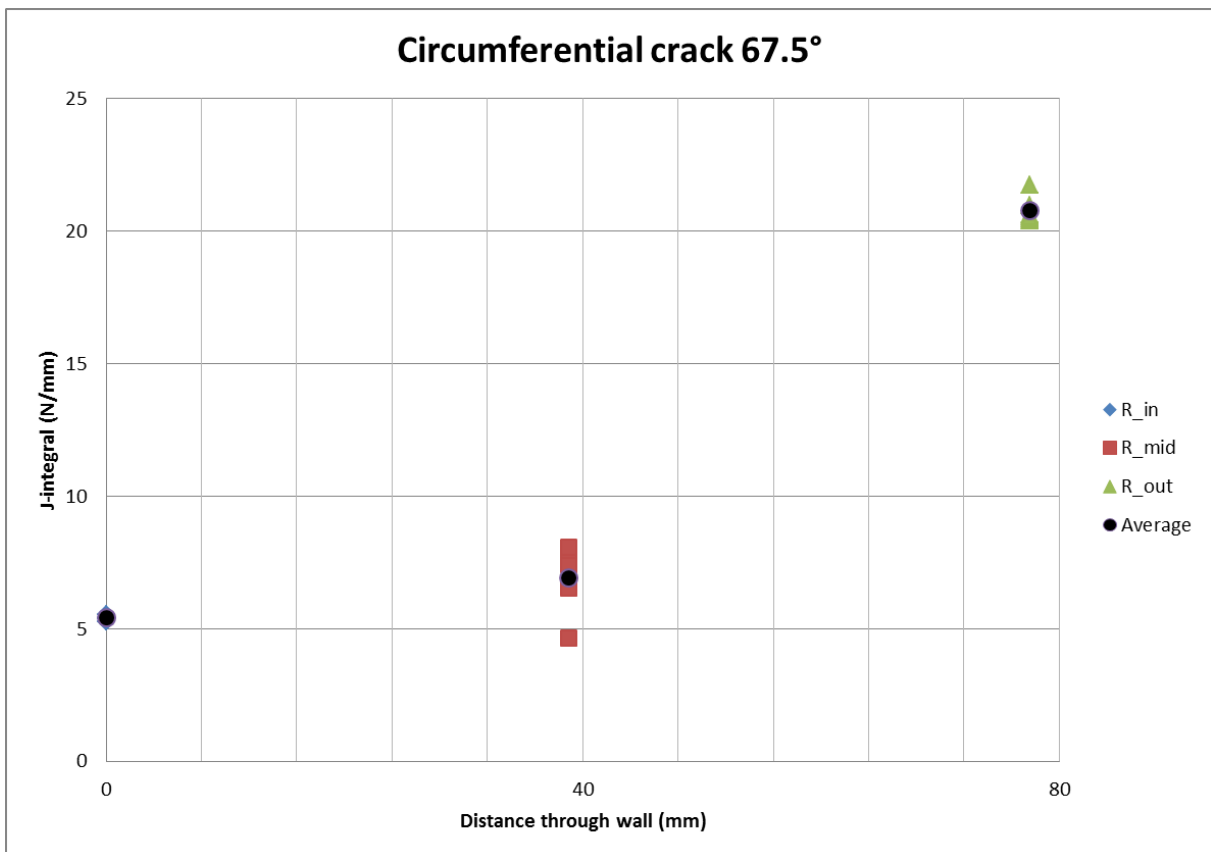


Figure 23. Calculated J-integrals from the $\theta=67.5^\circ$ crack.

A3. Crack opening displacements on crack edges

Local vertical displacements were determined from the finite analyses at the crack edges from both inner and outer sides. An example of an upper crack edge is shown in figure below for crack opening gap definition at the internal side (R_{in}).

Charts below show the vertical displacements at these edges on each crack case: 22.5°, 45° and 67.5°. Data obtained from the FE analyses were utilised for the leak rate calculation using SQUIRT2 code.

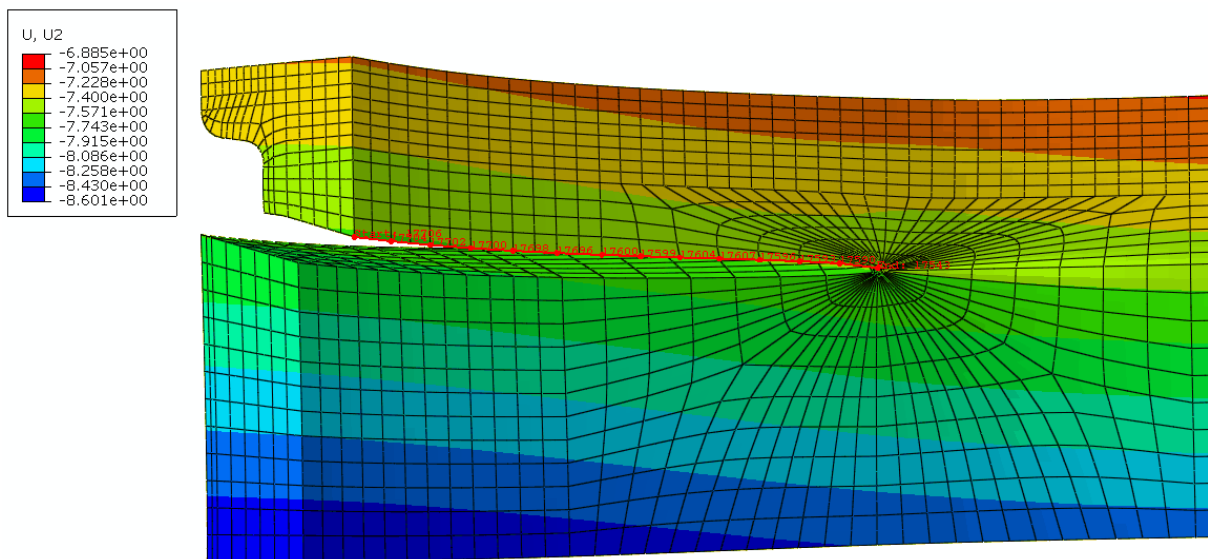


Figure 24. Vertical displacement distribution (in mm) at the crack vicinity and a chosen path for the crack gap definition at the crack upper edge.

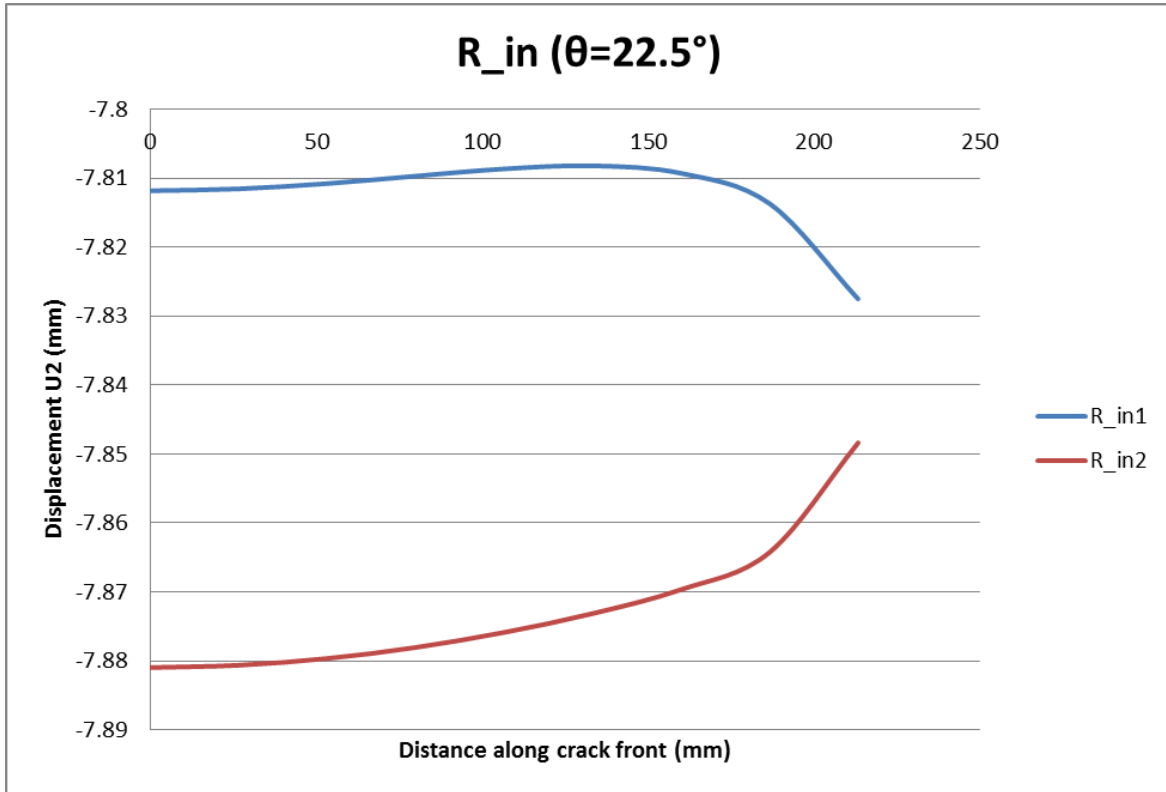
Crack 22.5°:


Figure 25. Vertical displacement distribution along upper and lower edges of the crack gap for the $\theta=22.5^\circ$ crack at the internal surface R_{in} .

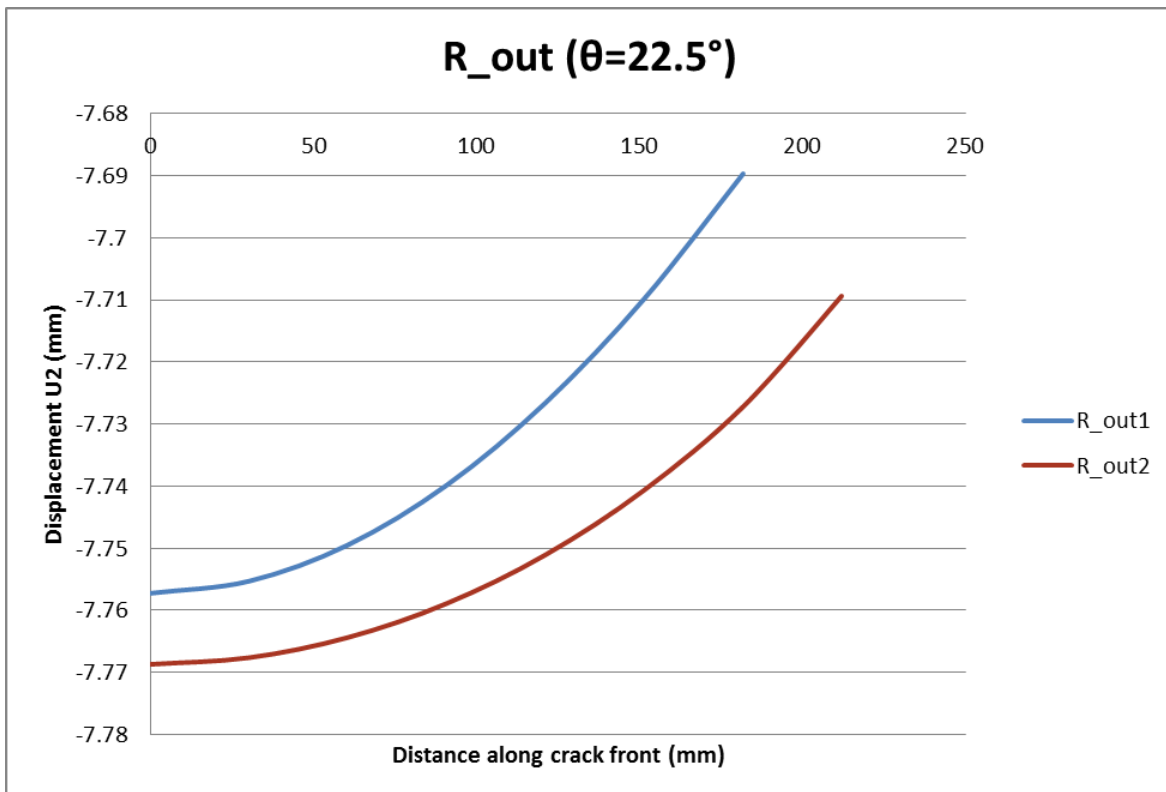


Figure 26. Vertical displacement distribution along upper and lower edges of the crack gap for the $\theta=22.5^\circ$ crack at the external surface R_{out} .

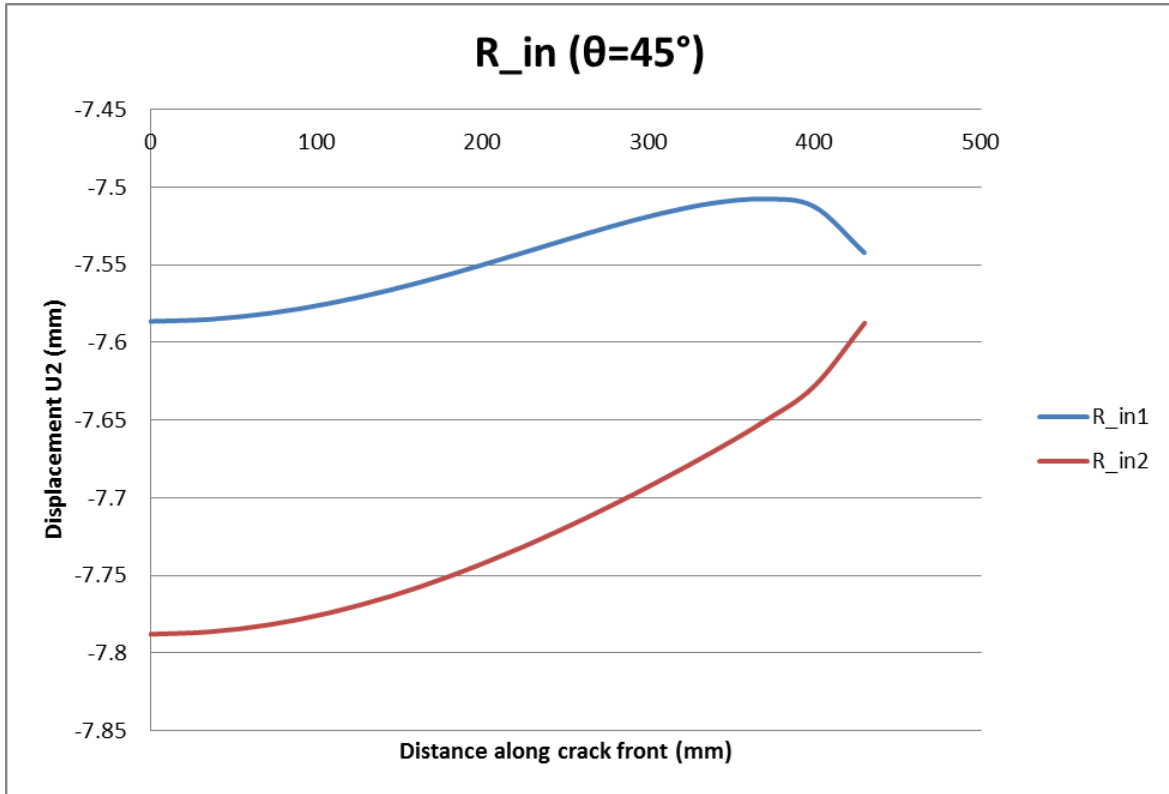
Crack 45°:


Figure 27. Vertical displacement distribution along upper and lower edges of the crack gap for the $\theta=45^\circ$ crack at the internal surface R_{in} .

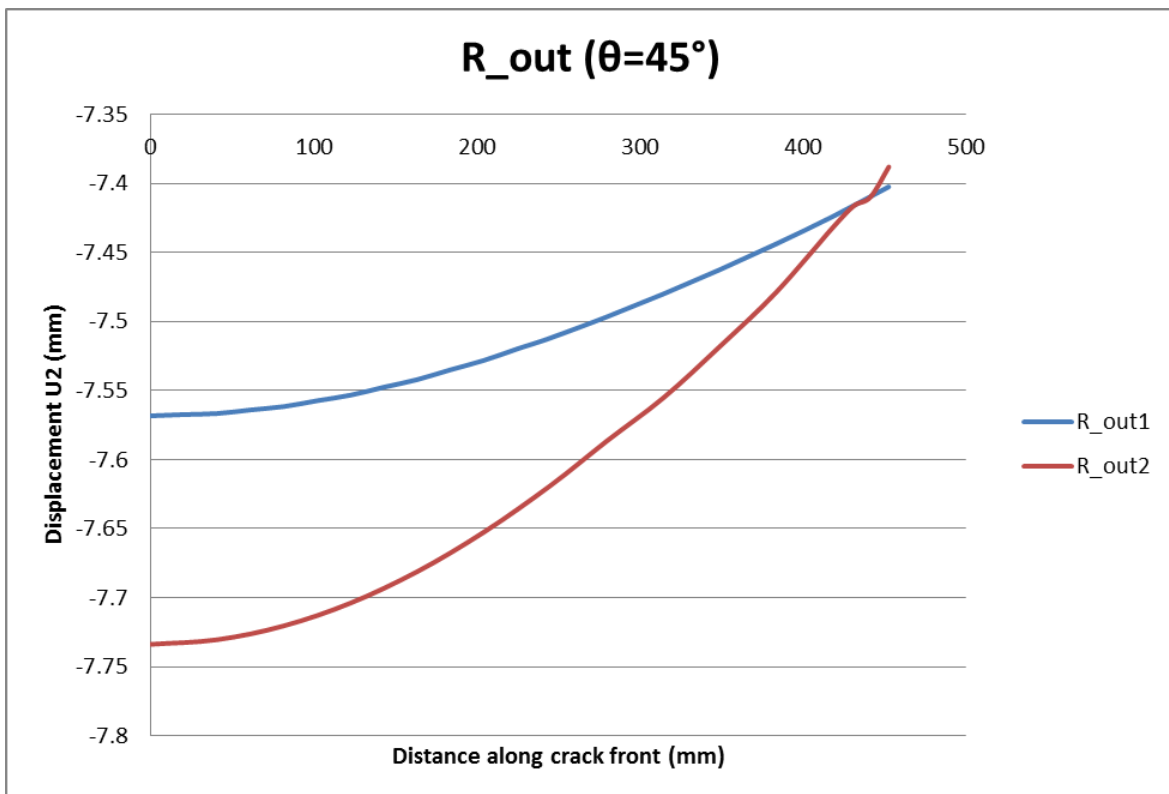


Figure 28. Vertical displacement distribution along upper and lower edges of the crack gap for the $\theta=45^\circ$ crack at the external surface R_{out} .

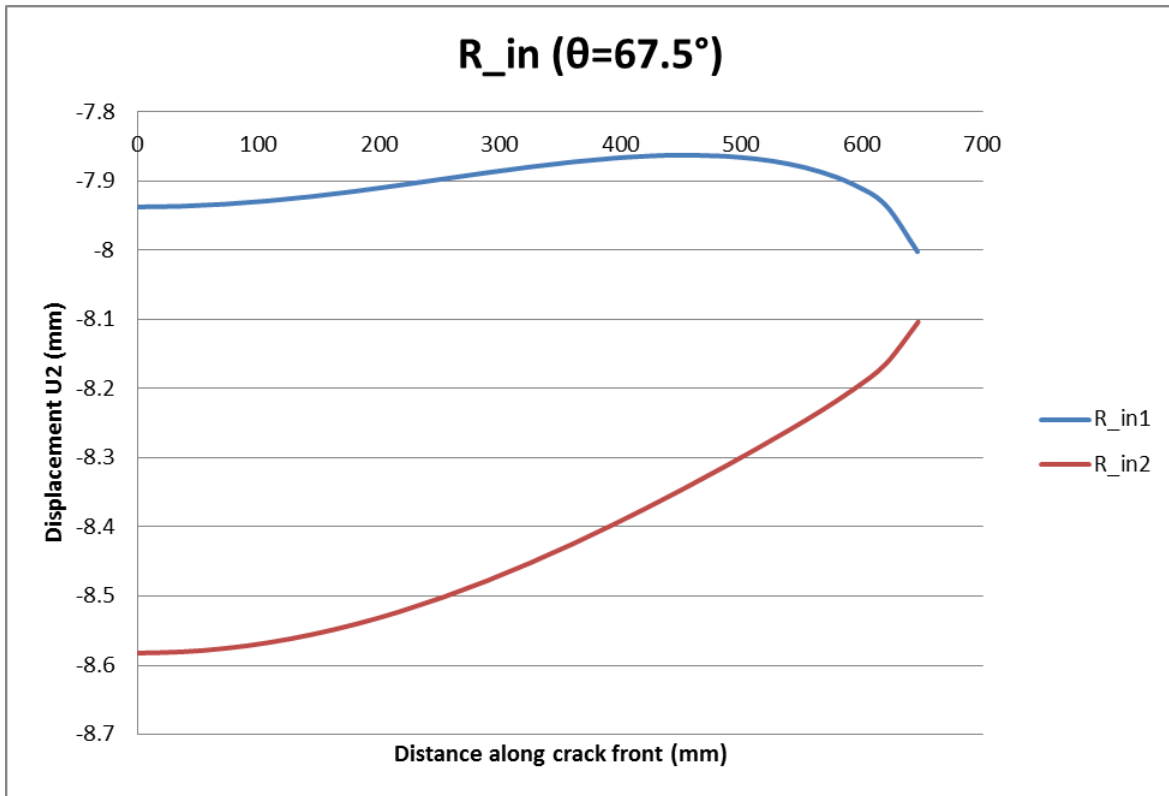
Crack 67.5°:


Figure 29. Vertical displacement distribution along upper and lower edges of the crack gap for the $\theta=67.5^\circ$ crack at the internal surface R_{in} .

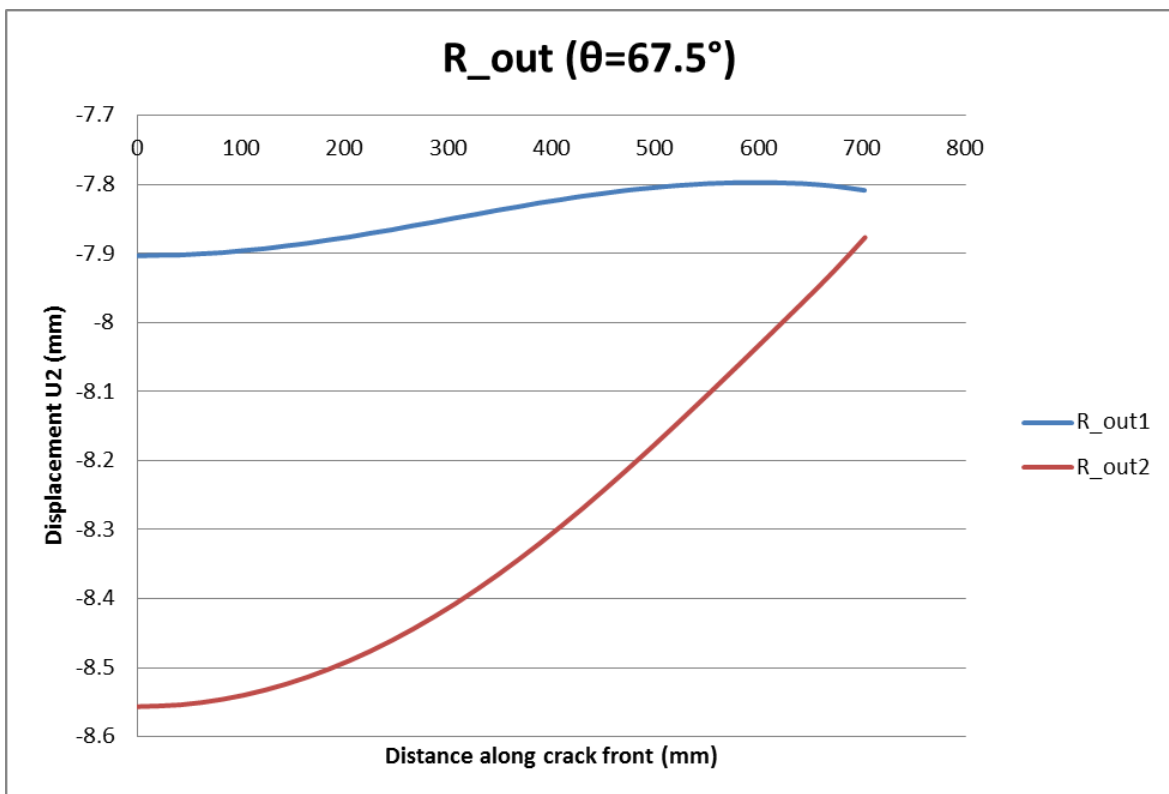


Figure 30. Vertical displacement distribution along upper and lower edges of the crack gap for the $\theta=67.5^\circ$ crack at the external surface R_{out} .